The Journal of Chemical Physics

Mapping wave packet bifurcation at a conical intersection in CH_3I by attosecond XUV transient absorption spectroscopy

Cite as: J. Chem. Phys. **154**, 234301 (2021); https://doi.org/10.1063/5.0056299
Submitted: 08 May 2021 . Accepted: 25 May 2021 . Published Online: 15 June 2021

Kristina F. Chang, Han Wang, Sonia M. Poullain, David Prendergast, Daniel M. Neumark, and Stephen R. Leone

COLLECTIONS

Paper published as part of the special topic on Special Collection in Honor of Women in Chemical Physics and Physical Chemistry

This paper was selected as Featured

This paper was selected as Scilight

View Online Export Citation CrossMark

ARTICLES YOU MAY BE INTERESTED IN

Real time mapping of methyl iodide dissociation at a conical intersection
Scilight **2021**, 251106 (2021); https://doi.org/10.1063/10.0005484

Multidimensional electronic spectroscopy in high-definition–Combining spectral, temporal, and spatial resolutions
The Journal of Chemical Physics **154**, 230901 (2021); https://doi.org/10.1063/5.0052234

Superposition-state N_2^+ produced in the intermolecular charge transfer from low-energy Ar^+ to N_2
The Journal of Chemical Physics **154**, 234303 (2021); https://doi.org/10.1063/5.0055002

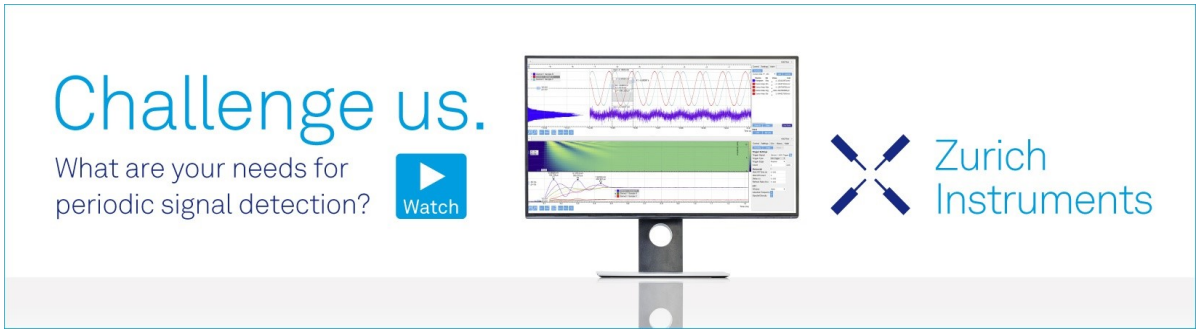

© 2021 Author(s).

The Journal of Chemical Physics ARTICLE scitation.org/journal/jcp

Mapping wave packet bifurcation at a conical intersection in CH_3I by attosecond XUV transient absorption spectroscopy

Cite as: J. Chem. Phys. 154, 234301 (2021); doi: 10.1063/5.0056299
Submitted: 8 May 2021 • Accepted: 25 May 2021 •
Published Online: 15 June 2021

View Online Export Citation CrossMark

Kristina F. Chang,[1] Han Wang,[2] Sonia M. Poullain,[3] David Prendergast,[2,4] Daniel M. Neumark,[1,2,a)] and Stephen R. Leone[1,2,5,b)]

AFFILIATIONS

[1] Department of Chemistry, University of California, Berkeley, California 94720, USA
[2] Chemical Sciences Division, Lawrence Berkeley National Laboratory, Berkeley, California 94720, USA
[3] Departamento de Química Física, Facultad de Ciencias Químicas, Universidad Complutense de Madrid, Madrid 28040, Spain
[4] Molecular Foundry, Lawrence Berkeley National Laboratory, Berkeley, California 94720, USA
[5] Department of Physics, University of California, Berkeley, California 94720, USA

Note: This paper is part of the JCP Special Collection in Honor of Women in Chemical Physics and Physical Chemistry.
[a)] **Electronic mail:** dneumark@berkeley.edu
[b)] **Author to whom correspondence should be addressed:** srl@berkeley.edu

ABSTRACT

Extreme ultraviolet (XUV) transient absorption spectroscopy has emerged as a sensitive tool for mapping the real-time structural and electronic evolution of molecules. Here, attosecond XUV transient absorption is used to track dynamics in the *A*-band of methyl iodide (CH_3I). Gaseous CH_3I molecules are excited to the *A*-band by a UV pump (277 nm, ~20 fs) and probed by attosecond XUV pulses targeting iodine I(4*d*) core-to-valence transitions. Owing to the excellent temporal resolution of the technique, passage through a conical intersection is mapped through spectral signatures of nonadiabatic wave packet bifurcation observed to occur at 15 ± 4 fs following UV photoexcitation. The observed XUV signatures and time dynamics are in agreement with previous simulations [H. Wang, M. Odelius, and D. Prendergast, J. Chem. Phys. **151**, 124106 (2019)]. Due to the short duration of the UV pump pulse, coherent vibrational motion in the CH_3I ground state along the C–I stretch mode (538 ± 7 cm^{-1}) launched by resonant impulsive stimulated Raman scattering and dynamics in multiphoton excited states of CH_3I are also detected.

Published under an exclusive license by AIP Publishing. https://doi.org/10.1063/5.0056299

I. INTRODUCTION

Attosecond and femtosecond core-to-valence absorption spectroscopy in the extreme ultraviolet (XUV) and x-ray regimes is a powerful means to follow electronic and structural changes associated with chemical reactions.[1–5] In core-to-valence absorption spectroscopy, transitions from element-specific core orbitals to valence orbitals are measured. The direct probing of the valence shell allows for excellent sensitivity to the bonding configuration and electronic state of the system. Combined with resonant pump pulses of few to tens-of-femtosecond duration, ultrafast XUV transient absorption spectroscopy offers a clear path for observing some of the fastest processes in photochemistry, including electronic state-switching dynamics at avoided crossings and conical intersections.[6,7] Here, we apply attosecond transient absorption spectroscopy to the UV-induced dissociation of CH_3I along the C–I bond, with the express goal of mapping wave packet dynamics through a conical intersection encountered during molecular fragmentation.

CH_3I has long been regarded as a prototype system for polyatomic photodissociation.[8–16] The *A*-band is accessed by I(5*p*) → σ^* excitation in the UV between 250 and 290 nm, comprising transitions to steeply repulsive electronic states that dissociate along the C–I bond. The optically allowed transitions in the *A*-band consist of two weak perpendicular transitions to $^3Q_1$ and $^1Q_1$ and one

Published under an exclusive license by AIP Publishing

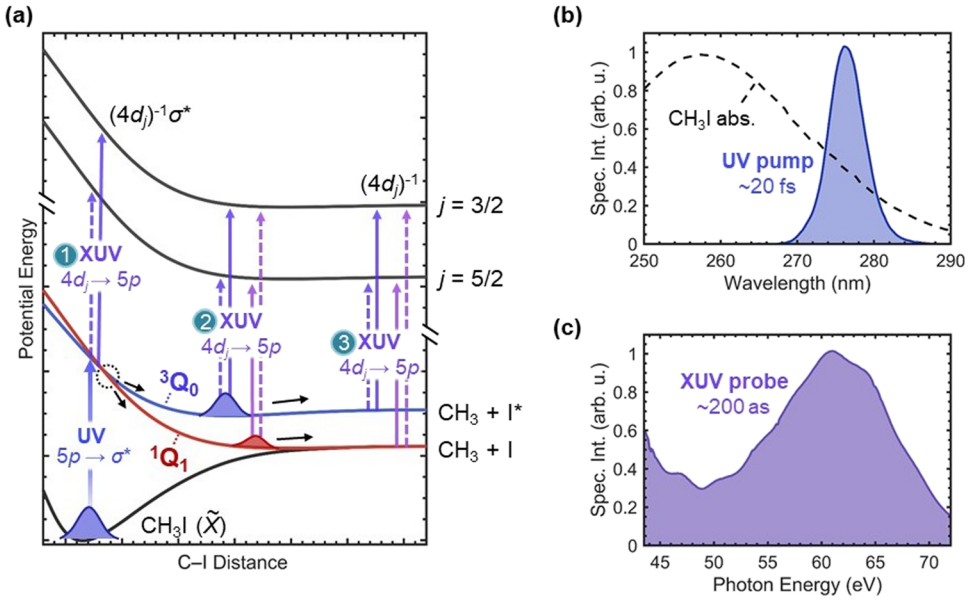

FIG. 1. Experimental pump–probe concept for the *A*-band photodissociation of CH_3I. (a) Relevant potential energy curves plotted schematically as a function of C–I distance. $^3Q_0$ (blue solid curve) is accessed from the ground state (black solid curve) by a UV pump (blue arrow). Wave packet bifurcation at a conical intersection (dashed circle) formed with $^1Q_1$ (red solid curve) governs the formation of atomic I and I* photoproducts from C–I dissociation. In this work, wave packet dynamics before the conical intersection (region 1), after the conical intersection (region 2), and in the dissociation limit (region 3) are mapped through XUV transitions to a pair of molecular $(4d_j)^{-1}\sigma^*$ core-excited states, correlating to atomic $(4d_j)^{-1}$ core-excited states at long C–I distances. Due to their antibonding character, the core-excited states are depicted as repulsive. In the schematic, strong and weak XUV transitions to the core-excited states are indicated using purple solid and dashed arrows, respectively. (b) UV pump pulse spectrum (blue shaded area) plotted in comparison to the previously reported absorption spectrum of CH_3I[23] (black dashed curve). (c) XUV probe pulse spectrum.

strong parallel transition to $^3Q_0$.[8,17] Due to nonadiabatic interactions between the predominantly excited $^3Q_0$ state and the $^1Q_1$ state, *A*-band dynamics following UV excitation primarily unfold along the $^3Q_0$ and $^1Q_1$ potentials. Excitation and dynamics due to $^3Q_1$ are expected to be minimal. As shown in the schematic in Fig. 1(a), UV excitation launches the majority of the excited wave packet on $^3Q_0$, initiating C–I dissociation to release spin–orbit excited $I^*(^2P_{1/2})$ atoms. However, a conical intersection encountered along the C–I bond length coordinate allows a portion of the wave packet to transfer to $^1Q_1$, leading to the production of ground state $I(^2P_{3/2})$ atoms. The photoproduct branching ratio resulting from the bifurcation of the initial $^3Q_0$ wave packet at this conical intersection has been estimated to be $I:I^* = 1:3$ following UV photoexcitation at 277 nm.[18] Based on *ab initio* molecular dynamics calculations, the $^3Q_0/^1Q_1$ conical intersection crossing is expected to occur on an exceedingly fast ~10 to 20 fs timescale, rendering direct experimental observations challenging.[16,19,20]

The photodissociation of CH_3I can be probed in the 40–60 eV spectral region of the XUV through iodine I(4*d*) core-to-valence absorption transitions. As shown in Fig. 1(a), dynamics along the *A*-band excited states can be spectroscopically followed with $4d \rightarrow 5p$ transitions localized on iodine along the reaction coordinate. Although CH_3I dissociation dynamics have been the subject of previous XUV transient absorption studies using this probing scheme,[21,22] the ~100 fs temporal resolution of those experiments precluded observations of sub-20 fs conical intersection dynamics.

In this study, ultrafast transient absorption spectroscopy is applied to the spectroscopic mapping of conical intersection dynamics through core-level I(4*d*) transitions in the XUV. The use of a considerably shorter, ~20 fs UV pump pulse enables wave packet bifurcation dynamics at the $^3Q_0/^1Q_1$ conical intersection to be resolved in time. In the experimental XUV spectra, passage through the conical intersection is identified via a signature of wave packet bifurcation along distinct valence-excited $^3Q_0$ and $^1Q_1$ states. The observed spectral signatures can be interpreted in a straightforward framework of I(4*d*) core-to-valence transitions and are verified by comparisons to simulated transient XUV spectra obtained in a previous computational study by Wang *et al.*[20] Finally, due to the short duration of the intense UV pump pulse, dynamics in multiphoton states and coherent vibrations in the CH_3I ground state launched by resonant impulsive Raman scattering are observed.

II. METHODS

A. Experimental methods

Liquid CH_3I (99.5% purity) was obtained from Sigma-Aldrich. The sample target consists of a 3 mm long gas flow cell filled to ~7 Torr of gaseous CH_3I at room temperature (298 K). The experimental laser setup utilizes femtosecond UV pump pulses and time-delayed attosecond XUV probe pulses focused into the sample gas cell to excite and probe dynamics in the CH_3I sample. The details of the instrumentation have been given previously.[24]

Published under an exclusive license by AIP Publishing

The experimental setup is based on the output of a Ti:sapphire amplifier, providing carrier-envelope phase-stable near-infrared (NIR) laser pulses (~780 nm, ~27 fs and 1.9 mJ, 1 kHz). The NIR pulses are spectrally broadened through self-phase modulation in a stretched hollow-core fiber (1.5 m long and 400 μm inner diameter) filled with 2.0 bars of neon gas. The spectrally broadened pulses span the visible to NIR wavelength range and are then compressed in time by a combination of chirped mirrors, a 2 mm thick ammonium dihydrogen phosphate crystal, and fused silica glass wedges. Following temporal compression, near transform-limited, few-cycle visible-NIR pulses (~550 to 950 nm, 3.8 fs, and 0.8 mJ) are obtained and subsequently used to drive the high harmonic generation of XUV pulses.[24] The few-cycle pulses are tightly focused into a high harmonic generation gas cell filled with flowing argon, producing ~200 as duration isolated attosecond XUV pulses via amplitude gating. The spectrum of the attosecond pulses exhibits a smooth continuum structure between 40 and 70 eV, as shown in Fig. 1(c). Residual light from the few-cycle driving pulse is removed from the XUV beam path by using a 300 nm thick aluminum filter. The XUV pulses are then focused by using a gold-coated toroidal mirror into the sample gas cell target, measuring characteristic I(4*d*) absorption resonances in the photon energy range between 44.0 and 60.0 eV.[7,21] The transmitted XUV spectrum is subsequently detected by using a home-built XUV spectrometer consisting of a concave grating and x-ray CCD camera. The energy resolution of the spectrometer is estimated to be ~25 meV.

Femtosecond UV pump pulses are generated by frequency tripling in beta barium borate (BBO) crystals. Frequency-doubling of a portion of the Ti:sapphire amplifier light in second harmonic generation BBO produces 30 fs, 400 nm pulses. The 400 nm pulses are mixed with 9 fs, 700–950 nm pulses isolated from the hollow-core fiber using a long-pass filter in 50 μm thick sum-frequency mixing BBO to produce UV pulses (277 nm center wavelength, 6 nm full width half maximum, and 19 fs transform-limited duration) and with pulse energies up to 9 μJ per pulse (9 mW average power at a 1 kHz repetition rate). The use of a free-standing BBO crystal for sum-frequency generation allows for the generation of significantly shorter, higher flux UV pump pulses compared to the previous setup.[7] In addition, the UV pulses are generated in vacuum, avoiding air dispersion during propagation of the pulses to the sample target. Following sum-frequency generation, residual 400 nm and 700–950 nm light is removed from the beam path using three reflective UV mirrors (R < 98% between 250 and 300 nm and T < 90% between 380 and 1000 nm).

At the sample gas cell, the UV pump beam is focused to a spot size of ~100 μm at a crossing angle of 0.7° with respect to the XUV beam. The UV beam after the sample cell is blocked before the x-ray CCD camera by using a 300 nm thick aluminum filter. A measurement of the UV-XUV instrument response function and the calibration of the pump–probe time delay are obtained using an *in situ* cross correlation measurement in atomic xenon.[7,21] With this methodology, an instrument response function of 24 ± 5 fs (full width at half maximum) and a 0 fs time delay calibration within an uncertainty of ±4 fs are determined. Due to the 0.7° crossing angle between the UV and XUV beams, the measured instrument response function is expected to be ~4 fs longer than UV pulse duration at the sample target. The UV pulse duration is therefore estimated to be 20 ± 5 fs *in situ*, corresponding to a near transform-limited pulse. In the current experiment, UV pump energies of 8.6 μJ per pulse are used, corresponding to an ~5×10^{12} W cm^{-2} peak intensity at the sample target. As shown in Fig. 1(b), the spectrum of the UV pump pulse lies within the absorption spectrum of CH_3I but is slightly detuned from the absorption band maximum located at ~260 nm.

Transient XUV absorption spectra are recorded as changes in optical density $\Delta OD = -\log[I_{XUV+UV}(E, \tau)/I_{XUV}(E)]$, where $I_{XUV+UV}(E, \tau)$ is the XUV spectrum recorded at the time delay τ following the UV pump and $I_{XUV}(E)$ is the XUV spectrum recorded in the absence of the pump. Each XUV spectrum is obtained from an average of 50 x-ray camera frames captured at an integration time of 1 s per frame. XUV spectra are collected at time delays between −60 and 300 fs at 4 fs intervals. To eliminate high-frequency noise, the recorded transients are post-processed using a low-pass Gaussian filter (see the supplementary material).

B. Theoretical methods

Simulated XUV transients corresponding to CH_3I dynamics in the *A*-band are obtained from a previous theoretical study by Wang *et al.*[20] Briefly, Tully's fewest-switches surface hopping (FSSH) approach[25] implemented within the SHARC software package was used to compute molecular trajectories starting on the $^3Q_0$ electronic state. The initial nuclear configurations of the trajectories are defined by a ground state Wigner distribution at 300 K. For each trajectory, transient XUV spectra based on $4d_j \rightarrow 5p$ transitions, where j = 5/2 and 3/2, were computed using the MS-CASPT2 method and ANO-RCC-VTZP basis set. The transients are summed in order to simulate an expected I:I* yield of 1:2 from ~277 nm excitation.[18] Finally, for comparison to the experimental results, the resulting simulation is temporally broadened by the experimental Gaussian instrument response.

III. RESULTS AND DISCUSSION

A two-dimensional colormap depicting transient XUV absorption spectrum of CH_3I between 44.0 and 54.0 eV is shown in Fig. 2. The transient represents the time-resolved probing of CH_3I molecular states and atomic photofragments through one-electron probing from the iodine 4*d* core orbital into unoccupied valence orbitals. The 49.5–54.0 eV spectral region of the transient is dominated by a pair of negative ΔOD features corresponding to the depletion of core-to-valence $4d_j \rightarrow \sigma^*$ transitions from the CH_3I ground state, where j = 3/2 and 5/2.[7,21,22] Meanwhile, the 44.0–49.5 eV spectral region is dominated by positive ΔOD features corresponding to the available $4d_j \rightarrow 5p$ transitions from molecular excited states and atomic photoproducts produced by the UV pump. Due to spin–orbit splitting of the $4d_j$ core level, $4d_j \rightarrow \sigma^*/5p$ transitions appear as a spin–orbit split pair of features in the XUV spectrum separated by ~1.7 eV.[26,27]

Between 49.5 and 54.0 eV (Fig. 2), oscillations in the $4d_j \rightarrow \sigma^*$ depletion features capture ground state wave packet dynamics launched by the UV pump. In addition, weak positive ΔOD features overlapping the depletion signals near 0 fs time delay are observed. The rise and decay of these signals closely follow the temporal profile of the experimental instrument response (see the supplementary material), which are assigned to an AC

Published under an exclusive license by AIP Publishing

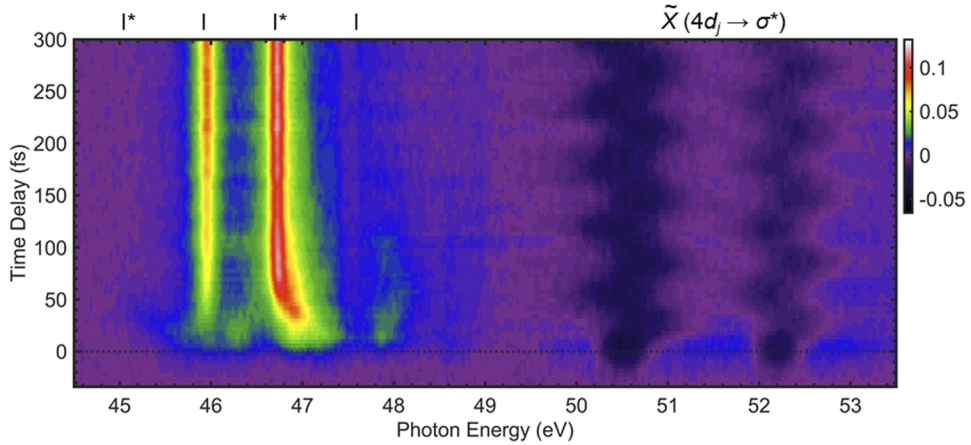

FIG. 2. Experimental transient XUV spectra of CH_3I plotted as a colormap. The colorscale of the transient corresponds to ΔOD. Between 44.5 and 49.5 eV, positive ΔOD features corresponding to molecular and atomic species produced by single or multiphoton UV pump excitation. The locations of the well-known atomic I(45.9, 47.6 eV) and I*(46.7 eV) transitions and a forbidden atomic I*(45.0 eV) transition are labeled above the transient. Between 49.5 and 54.0 eV, a pair of negative ΔOD features corresponding to $4d_j \rightarrow \sigma^*$ transitions from the CH_3I ground state are observed.

Stark effect[6,28] of the UV pulse electric field on the ground state resonances.

Between 44.0 and 49.5 eV, the evolution of molecular and atomic iodine $4d_j \rightarrow 5p$ features captures rapid *A*-band dissociation. C–I dissociation is evidenced through the appearance of the well-known core-to-valence transitions of atomic I and I*,[29] which dominate the transient. The atomic I signals consist of a strong transition at 45.9 eV [$I(^2P_{3/2} \rightarrow {}^2D_{5/2})$] and a weak transition at 47.6 eV [$I(^2P_{3/2} \rightarrow {}^2D_{3/2})$].[22] Meanwhile, the atomic I* signals consist of a strong transition at 46.7 eV [$I^*(^2P_{1/2} \rightarrow {}^2D_{3/2})$] and a forbidden transition at 45.0 eV [$I^*(^2P_{1/2} \rightarrow {}^2D_{5/2})$], which lies below the detection threshold of the experiment. The rise of the atomic I and I* signals at long time delays is indicative of C–I dissociation launched by the UV pump. At early time delays, the convergence of short-lived molecular features into the atomic iodine lines provides a mapping of C–I dissociation dynamics. Through comparisons to simulated XUV transients, the molecular features can be assigned to excited states accessed by single and multiphoton UV excitation.

The time-resolved probing of alkyl iodides by 4*d* core-to-valence transitions has been the subject of previous XUV transient absorption studies.[7,21,22,30] However, the use of 50 fs or longer UV pump pulses in the previous studies precluded the observation of several dynamics accessed in the current study. In particular, the use of significantly shorter ~20 fs UV pulses allows for the resolution of rapid CH_3I conical intersection dynamics during *A*-band dissociation and the launching of a coherent vibrational wave packet in the molecular ground state. In the following sections, we identify spectral signatures of *A*-band dynamics, separate these from the signals associated with multiphoton excitation, and analyze the launching mechanism of the ground state wave packet.

A. Direct mapping of conical intersection and dissociation dynamics in the *A*-band

The spectroscopic mapping of *A*-band dynamics in the experimental and simulated transients can be interpreted according to the UV pump–XUV probe scheme pictured in Fig. 1(a). In this scheme, *A*-band states are probed through doublet $4d_j \rightarrow 5p$ transitions in the XUV to a pair of spin–orbit split core-excited $(4d_j)^{-1}\sigma^*$ states, where j = 5/2 or 3/2. In the corresponding XUV absorption spectrum, $4d_{5/2} \rightarrow 5p$ transitions appear at lower photon energies relative to $4d_{3/2} \rightarrow 5p$ transitions. In the probing scheme [Fig. 1(a)], the preparation of a wave packet by direct UV photoexcitation to the Franck–Condon region (region 1) of $^3Q_0$ manifests in the appearance of a pair of $^3Q_0$ features at early time delays. At later time delays, bifurcation of the initial $^3Q_0$ wave packet following passage through the $^3Q_0/^1Q_1$ conical intersection is evidenced by a spectroscopic bifurcation of $^3Q_0$ (region 1) features into distinct $^3Q_0$ (region 2) and $^1Q_1$ (region 2) features. Finally, diabatic dissociation in the asymptotic region of the excited state potentials (region 3) is observed through the convergence of bifurcated $^3Q_0$ (region 2) and $^1Q_1$ (region 2) features in energy into purely atomic I* and I limits, respectively. The evolution of molecular features into atomic transitions is also accompanied by changes in intensity. Because atomic selection rules that govern the intensities of XUV transitions become increasingly relevant in the dissociation limit, spectral shifts of $^3Q_0$ (region 2) features into the forbidden atomic I*(45.0 eV) limit are correlated with a decay in signal intensity.

Figure 3(a) shows an expanded view of the experimental transient in the 44.0–49.5 eV spectral region. Signatures of dynamics launched by single-photon excitation can be identified through comparisons to a simulated transient representing CH_3I photodissociation in the *A*-band plotted in Fig. 3(b).[20] In particular, signatures of conical intersection and dissociation dynamics in the *A*-band in the experimental transient can be identified and distinguished from overlapping spectral features associated with multiphoton excitation. Spectral signatures characterizing the Franck–Condon region before the $^3Q_0/^1Q_1$ conical intersection (region 1), after the conical intersection (region 2), and in the dissociation limit (region 3) are labeled in the experimental and simulated transients [Figs. 3(a) and 3(b)]. Representative XUV spectra averaged over time delay ranges within regions 1–3 are also plotted in Figs. 3(c) and 3(d).

XUV spectra captured near 0 fs time delay characterize the Franck–Condon region (region 1). Averaged XUV spectra from −8 to 8 fs time delay characterizing molecular states accessed by direct UV excitation in the Franck–Condon region are plotted in Figs. 3(c) and 3(d). From a sum-of-Gaussians fitting, six distinct molecular signals can be identified in the experimental XUV

Published under an exclusive license by AIP Publishing

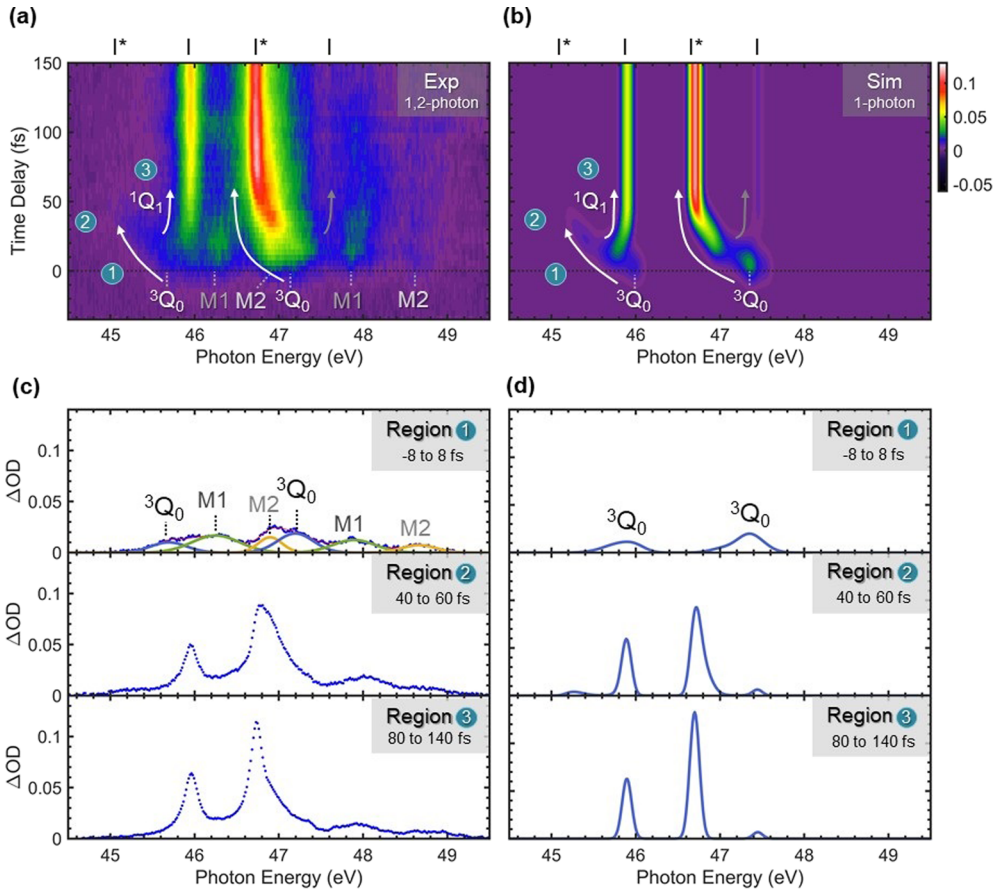

FIG. 3. Experimental and simulated transient spectra of CH_3I excited-state dynamics. (a) Experimental and (b) simulated spectra are plotted from 44.5 to 49.5 eV. Transients from −30 to 150 fs are plotted as a colormap and divided into dynamical regions before and after the conical intersection (regions 1–2) and in the dissociation limit (region 3). In the experimental and simulated transients, single-photon *A*-band dissociation manifests as sub-100 fs shifts of $^3Q_0$ and $^1Q_1$ signals into atomic I* and I limits. Experimentally observed shifts and theoretically expected shifts that are too weak to be observed are indicated using white and gray arrows, respectively. (c) Experimental and (d) simulated spectra captured over representative time delays. In the upper panels of (c) and (d), early time delay XUV spectra averaged between −8 and 8 fs characterize molecular states accessed directly by UV pump excitation before the conical intersection (region 1). Experimental data (blue circles) are fit to a sum of Gaussians (red solid curve), allowing for the identification of distinct molecular peaks (blue, green, and yellow solid curves). In addition to the $^3Q_0$ molecular state accessed by single-photon UV excitation, multiphoton excited molecular states, labeled M1 and M2, are observed in the experimental early time delay spectrum. In the lower panels of (c) and (d), representative XUV spectra characterizing temporal regions just after the conical intersection (region 2) and in the atomic I* and I dissociation limits (region 3) are shown.

spectrum [Fig. 3(c)]. As summarized in Table I, the molecular signals can be assigned to three pairs of ~1.7 eV split signals corresponding to $4d_j \rightarrow 5p$ transitions from three molecular excited states. Based on the comparison to the two spin–orbit split $^3Q_0$ features in the simulated XUV spectrum, the 45.7, 47.2 eV pair of signals is assigned to the $^3Q_0$ state in the *A*-band, which is dominantly accessed by single-photon UV excitation. Meanwhile, the 46.3, 47.9 eV pair and 46.9, 48.7 eV pair, labeled M1 and M2, respectively, are assigned to excited states beyond the *A*-band accessed by multiphoton UV excitation. The evolution of the observed multiphoton M1 and M2 features is discussed in detail in the supplementary material. An assignment of the multiphoton features to specific multiphoton excited states is not made at this time.

With spectral signatures of $^3Q_0$ excitation in the Franck–Condon region (region 1) assigned, we turn to the mapping of subsequent *A*-band dynamics following the $^3Q_0/^1Q_1$ conical intersection (region 2) and in the atomic I^* and I dissociation limits (region 3). As identified in Figs. 3(a) and 3(b), a pair of $^3Q_0$ (region 1) features appearing near 45.4 and 47.2 eV at 0 fs time delay in Figs. 3(a) and 3(b) captures the excitation of an initial $^3Q_0$ (region 1) wave packet through $4d_{5/2} \rightarrow 5p$ and $4d_{3/2} \rightarrow 5p$ transitions, respectively. In the 44.0–46.5 eV region of the transient associated with $4d_{5/2} \rightarrow 5p$ transitions from the *A*-band, the sub-20 fs division of the initial $^3Q_0$ (region 1) feature at 45.7 eV into two features is ascribed to a direct signature of wave packet bifurcation after the conical intersection into $^3Q_0$ and $^1Q_1$ (region 2). Within 100 fs, the bifurcated $^3Q_0$ and $^1Q_1$

Published under an exclusive license by AIP Publishing

TABLE I. Experimental peak positions and assignment of molecular signals identified in the 44.0–49.5 eV spectral region of the early time delay XUV spectrum averaged from −8 to 8 fs [Fig. 3(c), upper panel].

Molecular state assignment	UV excitation mechanism	XUV transition	Peak position (eV)	Energy splitting between peaks (eV)
$^3Q_0$	Single-photon	$4d_{5/2} \rightarrow 5p$ $4d_{3/2} \rightarrow 5p$	45.7 ± 0.1 47.2 ± 0.1	1.5 ± 0.2
M1	Multiphoton	$4d_{5/2} \rightarrow 5p$ $4d_{3/2} \rightarrow 5p$	46.3 ± 0.1 47.9 ± 0.1	1.6 ± 0.2
M2	Multiphoton	$4d_{5/2} \rightarrow 5p$ $4d_{3/2} \rightarrow 5p$	46.9 ± 0.1 48.7 ± 0.1	1.8 ± 0.2

features asymptotically evolve into respective atomic I*(45.0 eV) and I(45.9 eV) limits, capturing diabatic molecular dissociation along the C–I bond. The shift of the $^3Q_0$ (region 2) feature corresponding to $4d_{5/2} \rightarrow 5p$ transitions into the forbidden I*(45.0 eV) dissociation limit is accompanied by a complete decay in the intensity of the feature. Meanwhile, in the 46.5–49.5 eV region associated with $4d_{3/2} \rightarrow 5p$ transitions from the *A*-band, the shift of the $^3Q_0$ (region 1) feature at 47.2 eV into a prominent I*(46.7 eV) signal characterizes diabatic $^3Q_0$ dissociation dynamics. However, bifurcated $^1Q_1$ features converging toward the atomic I(47.6 eV) limit remain challenging to observe due overlapping M1 and M2 signals, precluding a clear mapping of conical intersection dynamics in this spectral region.

The experimental and simulated transients (Fig. 3) show strong qualitative agreement. However, the exact locations, widths, and signal intensities of XUV features deviate slightly. Deviations in the positions and widths of simulated spectral features from experimental results, especially at early time delays, could be partly explained by the neglected effects of the center wavelength and width of the UV pump spectrum on the position and distribution of the wave packet launched on $^3Q_0$ in the simulations. In addition, the simulations do not account for lifetime-broadening, leading to further deviations in the widths of computed XUV features from the experiment. Finally, a transient decrease in signal intensity at 47.2 eV along the shifting $^3Q_0$ feature in the simulation is not experimentally observed but may be partly obscured by an overlapping M2 signal in this spectral region.

Figure 4 shows an expanded view of the experimental and simulated transients in the 44.8–46.6 eV region where conical intersection dynamics are observed. In this spectral region, $^3Q_0$ wave packet bifurcation at the $^3Q_0/^1Q_1$ conical intersection is mapped to a u-shaped spectral feature bifurcating toward I*(45.0 eV) and I(45.9 eV) limits at long time delays. Points of maximum signal intensity along the feature are extracted as a function of photon energy and superimposed on the transients in Fig. 4. The minimum of the u-shaped spline trace (orange curve) along these points is interpreted as the temporal origin of the wave packet bifurcation event. From the experimental results, a bifurcation time of 15 ± 4 fs is determined. The reported uncertainty corresponds to the ±4 fs uncertainty in the calibrated zero time delay obtained using a cross correlation measurement in xenon. The experimental result is in close agreement with a simulated 13 fs conical intersection crossing time estimated from the FSSH molecular dynamics calculations used to produce the simulated CH_3I transients.[20] We note that this estimate also lies within the ~10 to 20 fs range of conical intersection crossing times estimated by other *ab initio* CH_3I dynamics calculations.[16,19,31,32]

The bifurcation signatures in Fig. 4 provide a direct characterization of $^3Q_0/^1Q_1$ conical intersection dynamics. In previous XUV transient absorption experiments on CH_3I,[21,22]

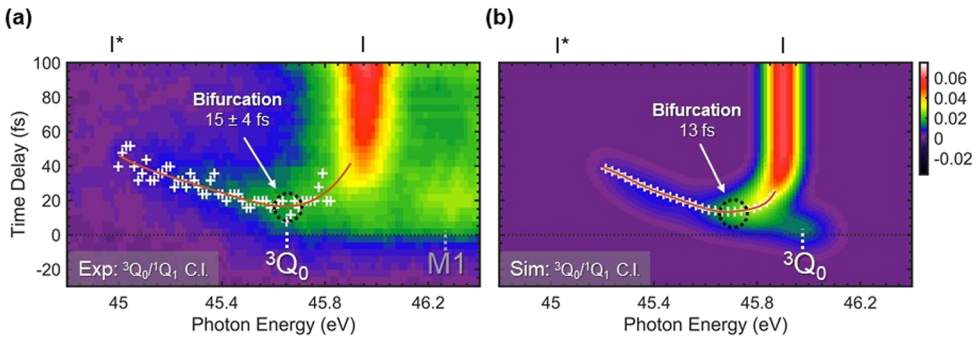

FIG. 4. Expanded view of conical intersection dynamics in the (a) experimental and (b) simulated CH_3I transients plotted from 44.8 to 46.6 eV. In this spectral region, XUV features are associated with $4d_{5/2} \rightarrow 5p$ transitions. Wave packet bifurcation at the $^3Q_0/^1Q_1$ conical intersection manifests as a u-shaped spectral feature. The bifurcation time is designated as the minimum of a spline trace (orange curve) along the intensity maxima (white + symbols) of the feature. The colorscale of the simulation in (b) is normalized to the colorscale of the experimental data in (a).

Published under an exclusive license by AIP Publishing

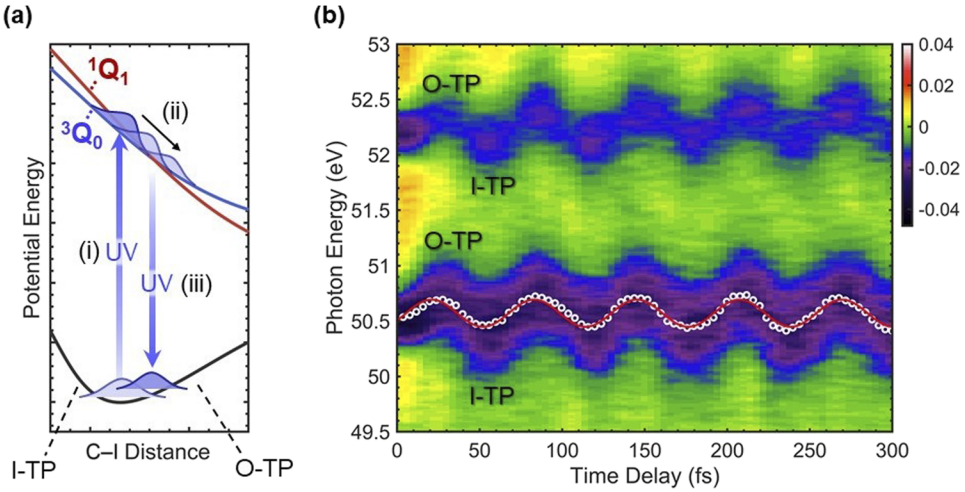

FIG. 5. Coherent vibrational dynamics in the CH_3I ground state. (a) Schematic of vibrational wave packet launching through a three-step resonant impulsive stimulated Raman process. (b) Transient map of ground state vibrational dynamics. The time-dependent peak positions of the ground state features (white circles) are fit to cosine functions (red curves). Inner and outer turning points of the vibrational wave packet are labeled I-TP and O-TP, respectively, in (a) and (b).

70–100 fs cross correlations precluded the observation of conical intersection dynamics. In recent transient absorption experiments on the *A*-band dynamics of larger alkyl iodides, *i*-C_3H_7I and *t*-C_4H_9I, electronic state-switching at the $^3Q_0/^1Q_1$ conical intersection was detected.[7] In the previous study, conical intersection dynamics were detected via the rise of $^1Q_1$ signals converging to the atomic I(45.9 eV) limit. However, due to the signal-to-noise ratio and cross correlation limitations, the significantly weaker $^3Q_0$ features converging to the forbidden I^*(45.0 eV) limit could not be detected. Here, the ability to fully map the passage through the conical intersection via $^3Q_0/^1Q_1$ bifurcation signatures converging to I^*(45.0 eV) and I(45.9 eV) atomic limits is attributed to the faster temporal resolution and signal-to-noise ratio of the experiment enabled by the use of UV pump pulses of shorter duration and higher flux.

B. Coherent vibrational motion in the ground state

In the experimental results (Fig. 2), cosinusoidal oscillations in the $4d_j \rightarrow \sigma^*$ depletion signals reflect coherent nuclear motion in the CH_3I ground state. With the use of a UV pump pulse shorter in duration than a typical ground state vibrational period, a coherent vibrational wave packet can be launched through an impulsive stimulated Raman scattering (ISRS) process.[33–36] Because the UV pump is resonant with electronic transitions between the ground state and $^3Q_0$ in the *A*-band, the Raman process becomes resonantly enhanced, leading to an appealing interpretation of ISRS in the framework of propagating wave packets. As plotted schematically in Fig. 5(a), resonant ISRS follows a three-step mechanism: (i) wave packet transfer from the ground state to an excited state surface by interaction with a resonant pulse, (ii) wave packet propagation on the excited state surface, and (iii) return of the excited state wave packet to the ground state via a second interaction with the resonant pulse. In step (iii), the scattering of a displaced wave packet from the excited state onto the ground state creates a coherent superposition of vibrational levels in the ground state, corresponding to a periodically oscillating wave packet. The composition of vibrational modes in the superposition reflects the vibrational activity of the molecule along the excited state in step (ii). Consequently, the highly active C–I stretch mode along the $^3Q_0$ surface is expected to appear in the ground state wave packet of CH_3I.

An expanded view of the oscillating $4d_j \rightarrow \sigma^*$ ground state features with an enhanced colorscale is shown in Fig. 5(b). Analysis of the frequency and phase of the cosinusoidal oscillations allows for the identification of the vibrational mode composition of the ground state wave packet and insight into its launching mechanism. To extract the dynamics of the ground state wave packet, we focus on analyzing the higher signal-to-noise feature between 49.5 and 51.5 eV corresponding to the $4d_{5/2} \rightarrow \sigma^*$ transition. The cosinusoidal oscillation of the feature is analyzed by modeling the spectral feature at each time point as a Gaussian and tracking its center position as a function of time delay. The oscillation of the peak position is modeled by a cosine function $E(\tau) = \Delta E \cos(\omega\tau + \varphi) + E_0$, from which an oscillatory frequency of $\omega = 538 \pm 7$ cm^{-1} corresponding to a vibrational period of $T = 62 \pm 1$ fs and a phase of $\varphi = (-0.74 \pm 0.06)\pi$ are extracted. The strong agreement between the measured frequency and the previously measured fundamental frequency of 533 cm^{-1} of the C–I stretch (ν_3) mode[37] suggests that the vibrational coherence mainly involves the $\nu = 0$ and 1 levels of ν_3, noting that coherences involving $\nu = 2$ and 3 levels will be anharmonically red-shifted to 518 cm^{-1}.[38] Finally, the corresponding phase of the oscillation, bounded by $-\pi > \varphi > -\pi/2$, indicates that the vibrational wave packet is launched *between* the outer turning point and the equilibrium position of the ground electronic state and undergoes an initial displacement toward larger C–I distances.[3] The involvement of the C–I stretch mode in the ground state vibrational wave packet and its measured phase are consistent with a resonant ISRS launching mechanism.

IV. CONCLUSIONS

Attosecond XUV absorption spectroscopy constitutes a powerful tool for revealing ultrafast conical intersection dynamics governing molecular reactions. In this study, a combination of femtosecond UV pump pulses and attosecond XUV probe pulses targeting I(4*d*) core-to-valence absorption transitions allows for

Published under an exclusive license by AIP Publishing

the real-time mapping of CH_3I dissociation through the $^3Q_0/^1Q_1$ conical intersection in the *A*-band. The sub-20 fs separation of a wave packet into distinct $^3Q_0$ and $^1Q_1$ electronic states at a conical intersection is resolved through a spectroscopic bifurcation of molecular features converging to atomic I^* and I signals in the dissociation limit. Signatures of *A*-band conical intersection dynamics and molecular fragmentation launched by single-photon excitation can be identified and distinguished from signatures of multiphoton states in the experimental transients through comparisons to a previous computational study. Finally, owing to the ultrashort duration of the UV pump pulse, a coherent vibrational wave packet launched by resonant ISRS along the C–I stretch coordinate in the CH_3I ground state is observed. The results highlight the capability of attosecond XUV transient absorption spectroscopy to capture electronic state-switching dynamics and coherent nuclear motion in polyatomic molecules.

SUPPLEMENTARY MATERIAL

See the supplementary material for the raw and post-processed CH_3I transient absorption spectra plotted over the full photon energy region recorded (44–60 eV), for an analysis of the AC Stark effect on the ground state CH_3I transient absorption features, and for a detailed discussion of the observed multiphoton features (M1 and M2) in the transient absorption spectra.

DEDICATION

This paper honors Eileen Spain for her contributions to undergraduate education in physical chemistry. As a Professor of Chemistry at Occidental College, Eileen has mentored and inspired many women, including one of the authors, to pursue careers in physical chemistry. Eileen is a recipient of the Cottrell Scholar Award and Henry Dreyfus Teacher-Scholar Award for excellence in academic leadership and education.

ACKNOWLEDGMENTS

This work was financed by the National Science Foundation (NSF) (Grant Nos. CHE-1951317 and CHE-1660417) (K.F.C. and S.R.L.) and by the U.S. Army Research Office (ARO) under Grant No. W911NF-14-1-0383 (K.F.C., D.M.N., and S.R.L.) and under Grant No. W011NF-20-1-0127 (K.F.C. and D.M.N.). Computational work was performed by H.W. and D.P., within the Gas Phase Chemical Physics Program through the Chemical Sciences Division of Lawrence Berkeley National Laboratory (LBNL) and supported by a user project at the Molecular Foundry, LBNL, both supported by the U.S. Department of Energy (DOE), Office of Science, Office of Basic Energy Sciences, under Contract No. DE-AC02-05CH11231. Supercomputer time was provided by the National Energy Research Scientific Computing Center. S.M.P. acknowledges funding from the European Union's Horizon 2020 Research and Innovation Program under the Marie Sklodowska-Curie grant agreement (Grant No. 842539, ATTOCONTROL). We also thank J. González-Vázquez for useful discussions.

DATA AVAILABILITY

The data that support the findings of this study are available from the corresponding author upon reasonable request.

REFERENCES

[1] A. R. Attar, A. Bhattacherjee, C. D. Pemmaraju, K. Schnorr, K. D. Closser, D. Prendergast, and S. R. Leone, Science **356**, 54 (2017).
[2] A. Bhattacherjee, C. D. Pemmaraju, K. Schnorr, A. R. Attar, and S. R. Leone, J. Am. Chem. Soc. **139**, 16576 (2017).
[3] Z. Wei, J. Li, L. Wang, S. T. See, M. H. Jhon, Y. Zhang, F. Shi, M. Yang, and Z.-H. Loh, Nat. Commun. **8**, 735 (2017).
[4] S. P. Neville, M. Chergui, A. Stolow, and M. S. Schuurman, Phys. Rev. Lett. **120**, 243001 (2018).
[5] H. Timmers, X. Zhu, Z. Li, Y. Kobayashi, M. Sabbar, M. Hollstein, M. Reduzzi, T. J. Martínez, D. M. Neumark, and S. R. Leone, Nat. Commun. **10**, 3133 (2019).
[6] Y. Kobayashi, K. F. Chang, T. Zeng, D. M. Neumark, and S. R. Leone, Science **365**, 79 (2019).
[7] K. F. Chang, M. Reduzzi, H. Wang, S. M. Poullain, Y. Kobayashi, L. Barreau, D. Prendergast, D. M. Neumark, and S. R. Leone, Nat. Commun. **11**, 4042 (2020).
[8] R. S. Mulliken, J. Chem. Phys. **8**, 382 (1940).
[9] S. J. Riley and K. R. Wilson, Faraday Discuss. Chem. Soc. **53**, 132 (1972).
[10] M. Shapiro and R. Bersohn, J. Chem. Phys. **73**, 3810 (1980).
[11] R. K. Sparks, K. Shobatake, L. R. Carlson, and Y. T. Lee, J. Chem. Phys. **75**, 3838 (1981).
[12] F. G. Godwin, P. A. Gorry, P. M. Hughes, D. Raybone, T. M. Watkinson, and J. C. Whitehead, Chem. Phys. Lett. **135**, 163 (1987).
[13] D. W. Chandler and P. L. Houston, J. Chem. Phys. **87**, 1445 (1987).
[14] A. T. J. B. Eppink and D. H. Parker, J. Chem. Phys. **110**, 832 (1999).
[15] M. E. Corrales, V. Loriot, G. Balerdi, J. González-Vázquez, R. de Nalda, L. Bañares, and A. H. Zewail, Phys. Chem. Chem. Phys. **16**, 8812 (2014).
[16] M. E. Corrales, J. González-Vázquez, R. de Nalda, and L. Bañares, J. Phys. Chem. Lett. **10**, 138 (2019).
[17] A. Gedanken and M. D. Rowe, Chem. Phys. Lett. **34**, 39 (1975).
[18] D. Zhong and A. H. Zewail, J. Phys. Chem. A **102**, 4031 (1998).
[19] H. Guo, K. Q. Lao, G. C. Schatz, and A. D. Hammerich, J. Chem. Phys. **94**, 6562 (1991).
[20] H. Wang, M. Odelius, and D. Prendergast, J. Chem. Phys. **151**, 124106 (2019).
[21] A. R. Attar, A. Bhattacherjee, and S. R. Leone, J. Phys. Chem. Lett. **6**, 5072 (2015).
[22] L. Drescher, M. C. E. Galbraith, G. Reitsma, J. Dura, N. Zhavoronkov, S. Patchkovskii, M. J. J. Vrakking, and J. Mikosch, J. Chem. Phys. **145**, 011101 (2016).
[23] C. M. Roehi, J. B. Burkholder, G. K. Moortgat, A. R. Ravishankara, and P. J. Crutze, J. Geophys. Res. **102**, 12819, https://doi.org/10.1029/97jd00530 (1997).
[24] H. Timmers, Y. Kobayashi, K. F. Chang, M. Reduzzi, D. M. Neumark, and S. R. Leone, Opt. Lett. **42**, 811 (2017).
[25] J. C. Tully, J. Chem. Phys. **93**, 1061 (1990).
[26] G. O'Sullivan, J. Phys. B: At. Mol. Phys. **15**, L327 (1982).
[27] T. N. Olney, G. Cooper, and C. E. Brion, Chem. Phys. **232**, 211 (1998).
[28] E. R. Warrick, W. Cao, D. M. Neumark, and S. R. Leone, J. Phys. Chem. A **120**, 3165 (2016).
[29] G. O'Sullivan, C. McGuinness, J. T. Costello, E. T. Kennedy, and B. Weinmann, Phys. Rev. A **53**, 3211 (1996).
[30] A. Bhattacherjee, A. R. Attar, and S. R. Leone, J. Chem. Phys. **144**, 124311 (2016).
[31] A. B. Alekseyev, H.-P. Liebermann, R. J. Buenker, and S. N. Yurchenko, J. Chem. Phys. **126**, 234102 (2007).
[32] M. Kamiya and T. Taketsugu, J. Comput. Chem. **40**, 456 (2019).
[33] Y. X. Yan, E. B. Gamble, and K. A. Nelson, J. Chem. Phys. **83**, 5391 (1985).
[34] U. Banin, A. Bartana, S. Ruhman, and R. Kosloff, J. Chem. Phys. **101**, 8461 (1994).
[35] L. Dhar, J. A. Rogers, and K. A. Nelson, Chem. Rev. **94**, 157 (1994).
[36] M. T. Zanni, B. J. Greenblatt, A. V. Davis, and D. M. Neumark, J. Chem. Phys. **111**, 2991 (1999).
[37] T. Shimanouchi, *Tables of Molecular Vibrational Frequencies* (National Bureau of Standards, 1972), Vol. I.
[38] J. L. Duncan, A. M. Ferguson, and S. Mathews, J. Chem. Phys. **91**, 783 (1989).

Published under an exclusive license by AIP Publishing